Copyrights IEEE 2015

Fixed-structure feedforward control law for minimum- and nonminimum-phase LTI SISO systems

Maciej Marcin Michałek, *Member, IEEE*,

***Abstract*—Fundamental limitation of the model-inverse feedforward control results from instability or non-causality of the inverse of nonminimum-phase dynamics which cannot be applied in practice. To overcome this limitation, the approximate-inverse methods have been proposed in the literature. Structures of feedforward controllers proposed so far highly depend on a plant model structure. Therefore in general, their implementation may be inconvenient or troublesome in industrial applications. In this context, a simple fixed-structure feedforward control law is proposed in this paper in a form of a weighted linear combination of a reference trajectory and its time-derivatives. Design rules for selection of the weights are derived and provided in an explicit (analytical) form. The proposed control law can be employed to both nonminimum- and minimum-phase LTI SISO systems. The new method has been compared with classical feedforward controllers known from the literature revealing its advantages and limitations. Results of numerical examples and experimental validation tests obtained for an electronic plant have been reported.**

***Index Terms*—feedforward control design, trajectory tracking, nonminimum-phase dynamics, linear systems**

I. Introduction

LET us consider an LTI SISO plant, with input $u(t)$ and output $y(t)$, represented by the transfer function

$$G(s) \triangleq \frac{Y(s)}{U(s)} = \frac{b_m s^m + \ldots + b_1 s + b_0}{a_n s^n + \ldots + a_1 s + a_0} = \frac{B(s)}{A(s)} \quad (1)$$

with $b_0 \neq 0$. Model (1) covers both stable/unstable and minimum-phase/nonminimum-phase dynamics. The problem under consideration concerns feedforward control design for system (1) in the two-degrees-of-freedom (2DOF) tracking control system. In the literature, one distinguishes two alternative 2DOF control structures: with the *plant-inversion* feedforward and with the *closed-loop-inversion* feedforward. In the paper, an attention will be mostly paid on the former structure presented in Fig. 1, where y_d denotes a sufficiently smooth reference trajectory, $G_R(s)$ is a stabilizing controller, and e is a tracking error

$$e(t) \triangleq y_d(t) - y(t). \quad (2)$$

The plant-inversion feedforward has several important properties discussed e.g. in [7] and has been widely utilized in industrial applications, [8], [21]. One particular advantage of the control system structure with plant-inversion feedforward, which motivated its selection for further considerations, is an independence of a feedforward design process from dynamics of a stabilizing controller.

Various approaches to feedforward control design have been proposed in the literature, see e.g. [2], [5], [12], [14], [20] and the review papers [7], [21]. The classical model-inverse approach, applied in the control system from Fig. 1, employs a feedforward controller $G_{\mathrm{FF}}(s)$ equal to an inverse $G^{-1}(s)$ of plant dynamics. It has been shown in [8] that the feedforward control designed in this way improves output-tracking performance relative to a pure feedback control if a plant-model uncertainty is sufficiently small (at least over some frequency range of interest). The model-inverse strategy, however, has a

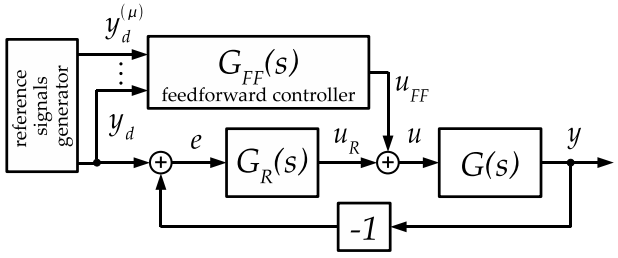

Fig. 1. The 2DOF control system with the plant-inversion feedforward.

fundamental limitation, since $G_{\mathrm{FF}}(s) = G^{-1}(s)$ is practically applicable only if the system (1) is minimum-phase, that is when all the roots of numerator polynomial of (1) lie in the left-half complex plane [13]. To overcome this limitation, two alternative general classes of feedforward design methods have been proposed in the literature for the nonminimum-phase plants: preview-based methods and approximate-inverse methods. Control laws from the former class (see e.g. [26], [27], and [15]) employ the preview information about a reference trajectory which must be available sufficiently early prior to its application in the control system. Methods from the second class try to approximate the unstable exact inverse of the plant model by some stable transfer function. In this paper, we are mostly interested in the approximate-inverse methods which are relatively simple and require only current values of the reference signal and its time-derivatives (see [4] and [7], [21]). In this class, three classical concepts have been proposed: the nonminimum-phase zero ignore (NZI), the zero-magnitude error (ZME), and the zero-phase error (ZPE) methods (various extensions or modifications of them can be found in [6], [11], [19], [23], [24]). Origins of the classical

The author is with the Chair of Control and Systems Engineering, Poznan University of Technology (PUT), Piotrowo 3a, 60-965 Poznań, Poland, e-mail: maciej.michalek@put.poznan.pl

methods naturally come from the frequency domain analysis. As a consequence, a structure and effectiveness of the classical approximate-inverse feedforward controllers generally depend on a particular structure and quantitative characteristics of a plant transfer function [4].

The aim of this work is to provide simple rules of feedforward control design for dynamics (1) in a form of the linear combination of a reference trajectory and its successive time-derivatives

$$u_{\text{FF}}(t) \triangleq p_\mu y_d^{(\mu)}(t) + \ldots + p_1 y_d^{(1)}(t) + p_0 y_d(t), \quad (3)$$

where $\mu \in \mathbb{N}$ and $p_\mu, \ldots, p_0 \in \mathbb{R}$ are treated as design parameters. Selection of coefficients $p_\mu, \ldots, p_0$ proposed in the paper takes into account not only poles of the plant dynamics but also allows compensating for the influence of a time-delay and plant zeros, regardless of their location in the open left- or right-half complex plane. The main reason for proposing the fixed-structure feedforward (3) comes from its simplicity, especially in the context of its practical implementation.

The design approach presented in this paper is a frequency-domain generalization of the idea based on a simple time-domain analysis of plant dynamics presented in the preliminary work [9]. For the sake of conciseness, the time-domain analysis is not continued here. Instead, the feedforward design rules are derived completely in a frequency domain, which provides more insight into benefits and limitations of the new method, and permits its direct comparison with the classical feedforward methods known from the literature.

Application of a fixed-structure feedforward is not a completely new idea. A feedforward control law similar to (3) for the special case of $\mu = 4$ has been proposed for the class of electromechanical servo systems in [25] (see also references cited therein). The method presented in this paper generalizes the concept of a fixed-structure feedforward to a wider class of systems represented by (1), and provides explicit analytical equations for the coefficients of a linear combination in (3). Furthermore, the proposed method has been qualitatively and quantitatively compared with the NZI, ZME, and ZPE control laws revealing conditions under which the new method outperforms the classical ones in the context of obtainable ultimate output-tracking performance.

II. System description and assumptions

We formulate two essential assumptions related to system (1) required for further considerations.

A1. Dynamics (1) is at least proper ($n \geq m$), is perfectly known, and the numerator and denominator polynomials of (1) do not have any common factors.

A2. Polynomial $B(s)$ is such that $B(0) = b_0 = 1$, and can be factorized as follows

$$B(s) = B^p(s)B^n(s), \quad (4)$$

where

$$B^p(s) = \beta_\gamma s^\gamma + \ldots + \beta_1 s + 1, \quad \gamma \leq m, \quad (5)$$

$$B^n(s) = \alpha_\lambda s^\lambda + \ldots + \alpha_1 s + 1, \quad \lambda \leq m, \quad (6)$$

with $\gamma + \lambda = m$, represent polynomials with roots having solely strictly positive or strictly negative real parts, respectively (no roots on the imaginary axis).

Perfect knowledge of the plant dynamics assumed in A1 indicates that we address a nominal feedforward control design, where any parametric uncertainty is not considered. Assumption A2 does not reduce generality of model (1). In the case when $B(0) \neq 1$, one can simply divide numerator and denominator of (1) by b_0 to meet A2.

Remark 1: In a more general case, the plant dynamics is usually described by the transfer function

$$G(s) = \frac{D(s)}{C(s)} \exp(-sT_0), \quad (7)$$

where $C(s) = c_{n_c} s^{n_c} + \ldots + c_1 s + c_0$, $D(s) = d_{m_d} s^{m_d} + \ldots + d_1 s + d_0$, $\deg C(s) = n_c \geq \deg D(s) = m_d$, while $T_0 > 0$ represents a time-delay. The required rational form of transfer function (1) can be obtained in this case by approximating the time-delay term of (7) with one of three most popular ν-order rational approximations:

$$\exp(-sT_0) \approx \frac{1}{q_\nu s^\nu + \ldots q_1 s + 1}, \quad q_i = \frac{T_0^i}{i!}, \quad (8)$$

$$\exp(-sT_0) \approx 1 + q_1 s + \ldots + q_\nu s^\nu, \quad q_i = \frac{(-T_0)^i}{i!}, \quad (9)$$

$$\exp(-sT_0) \approx \frac{(1 - T_0 s/2\nu)^\nu}{(1 + T_0 s/2\nu)^\nu}, \quad \nu \in \mathbb{N}, \quad (10)$$

where the latter one is called the ν-order Padé approximation. The effect of the above approximation on resultant control performance achievable with feedforward control law (3) will be illustrated in Section V-A.

For the purpose of further analysis let us define three characteristic transfer functions:

$$G_R(s) \triangleq \frac{U_R(s)}{E(s)} = \frac{l_r s^r + \ldots + l_1 s + l_0}{M_k s^k + \ldots + M_1 s + M_0} = \frac{L(s)}{M(s)},$$

$$G_{\text{FF}}(s) \triangleq \frac{U_{\text{FF}}(s)}{Y_d(s)} \overset{(3)}{=} P(s) = p_\mu s^\mu + \ldots + p_1 s + p_0, \quad (11)$$

$$G_E(s) \triangleq \frac{E(s)}{Y_d(s)} = \frac{1 - G(s)G_{\text{FF}}(s)}{1 + G(s)G_R(s)} \quad (12)$$

$$= S(s)[1 - G(s)G_{\text{FF}}(s)] = S(s)\Gamma(s) \quad (13)$$

which represent, respectively, dynamics of the stabilizing controller, the fixed-structure feedforward controller for $\mu \geq n$, and dynamics of the *error transfer function*. $S(s)$ introduced in (13) is a closed-loop sensitivity function, while $\Gamma(s)$ represents the *feedforward mismatch* transfer function such that

$$\Gamma(s) \equiv 0 \quad \Leftrightarrow \quad G_{\text{FF}}(s) \triangleq G^{-1}(s). \quad (14)$$

Satisfaction of (14) guarantees a zero steady-state tracking error in a response to reference trajectory $y_d(t)$. Thus, relation (14) reflects a nominal case of feedforward control design, which is practically feasible if $G^{-1}(s)$ is stable and causal. It is well known that (14) is not acceptable when the transfer function $G(s)$ is nonminimum-phase.

Let us complement assumptions A1-A2 with two additional prerequisites related to the control system presented in Fig. 1.

A3. $G_R(s)$ is a stabilizing controller for system (1) guaranteeing stability of the closed-loop system from Fig. 1 with $u_{\text{FF}} = 0$, that is, all the poles of error transfer function (12) are located in the open left-half complex plane.

A4. The reference trajectory $y_d(t) : \mathbb{R}_{\geq 0} \mapsto \mathbb{R}$ is a bounded continuous-time function of class $\mathcal{C}^\mu$ with sufficiently high $\mu \geq 1$. Moreover, $y_d(t)$ as well as its successive time-derivatives $y_d^{(1)}(t), \ldots, y_d^{(\mu)}(t)$ are perfectly known at any current time instant $t \geq 0$.

Assumption A3 permits the plant dynamics to be only marginally stable or even unstable. Assumption A4 ensures that time-derivatives $y_d^{(1)}(t), \ldots, y_d^{(\mu)}(t)$ exist, are bounded, and all the reference signals $y_d(t), y_d^{(1)}(t), \ldots, y_d^{(\mu)}(t)$ are not corrupted by noise (nominal case) being available with sufficient precision at every current time instant.

Remark 2: Requirements determined by A4 are common in the literature addressing feedforward design for the continuous-time systems in the context of *trajectory tracking* control problem[1] (see e.g. [5], [6], [24], [26]). They correspond to sufficient smoothness of a reference trajectory. In the particular case of only piecewise constant reference signal (often encountered in industrial applications), which shall be treated rather as a *degenerated trajectory*, one can meet assumption A4 by preliminary *smoothing* the reference signal passing it through a low-pass filter of sufficiently high dynamics order. If this additional complexity is not acceptable from any reasons, one can eventually treat the piecewise constant reference signal as *almost satisfying* assumption A4 by taking $y_d^{(\mu)}(t) = \ldots = y_d^{(1)}(t) \equiv 0$ (that is, by omitting a zero-measure set of Dirac deltas).

III. Feedforward design in a frequency domain

We are going to investigate how the nominal design strategy (14) can be approximated by application of the fixed-structure feedforward control law defined by (3). The way of approximation proposed in the sequel will determine a unified approach to a bounded feedforward control design for both minimum- and nonminimum-phase systems.

A. Characteristic transfer functions for $G_{FF} \triangleq P(s)$

The error transfer function (12) in the case of feedforward control law (11) takes the following form

$$G_E(s) = \frac{M(s)[A(s) - B(s)P(s)]}{M(s)A(s) + B(s)L(s)} = \frac{M(s)W(s)}{H(s)}, \quad (15)$$

where – upon assumption A3 – it is guaranteed that characteristic equation $H(s) = 0$ has all the roots in the open left-half complex plane. Polynomial $W(s) = A(s) - B(s)P(s)$ can be expressed in the detailed form as

$$W(s) = \sum_{j=0}^{n} a_j s^j - \sum_{i=0}^{m}\sum_{j=0}^{\mu} b_i p_j s^{j+i} = \breve{W}(s) + \tilde{W}(s), \quad (16)$$

where

$$\breve{W}(s) = w_{\mu+m}s^{\mu+m} + \ldots + w_{n+1}s^{n+1}, \quad (17)$$

$$\tilde{W}(s) = w_n s^n + \ldots + w_1 s + w_0, \quad (18)$$

with coefficients

$$w_0 = a_0 - b_0 p_0, \quad (19)$$

$$w_j = a_j - b_0 p_j - \sum_{i=1}^{j} b_i p_{j-i}, \quad j \in \{1, \ldots, \mu + m\}, \quad (20)$$

taking $a_j = 0$ for $j > n$, $b_i = 0$ for $i > m$, and $p_{j-i} = 0$ for $j - i > \mu$. Now, according to (16), one can write $P(s) = [A(s) - \breve{W}(s) - \tilde{W}(s)]/B(s)$, and the mismatch transfer function takes the form:

$$\Gamma(s) \overset{(13)}{=} 1 - G(s)G_{\text{FF}}(s) \overset{(11)}{=} 1 - \frac{B(s)}{A(s)}P(s) \overset{(15)}{=} \frac{W(s)}{A(s)} \overset{(16)}{=} \frac{\breve{W}(s) + \tilde{W}(s)}{A(s)}. \quad (21)$$

Since the sensitivity function $S(s)$ in (13) does not depend on a feedforward controller, the tracking error can be decreased – at least over some finite frequency range which covers a spectrum of reference signal y_d – by decreasing the module $|\Gamma(\bar{j}\omega)|$ through appropriate design of coefficients of polynomial $P(s)$ (note: $\bar{j} \triangleq \sqrt{-1}$).

B. The new approximate-inverse feedforward control law

Let us assume first that the degree of polynomial $P(s)$ results from the order of plant dynamics, that is $\mu = n$. In this case, one can directly influence the first $n+1$ coefficients of polynomial $W(s)$ in (16). In particular, one can remove polynomial $\tilde{W}(s)$ from mismatch transfer function (21) by designing coefficients p_0 to p_n such that $w_0 = \ldots = w_n = 0$. According to equations (19)-(20), and under assumption A2, it leads to the following recursive design formulas:

$$p_0 \triangleq a_0, \quad (22)$$

$$p_j \triangleq a_j - \sum_{i=1}^{j} b_i p_{j-i} \quad \text{for} \quad j \in \{1, \ldots, n\}. \quad (23)$$

As a consequence, the feedforward control law

$$u_{\text{FF}}^{\text{CAI}}(t) \triangleq p_n y_d^{(n)}(t) + \ldots + p_1 y_d^{(1)}(t) + p_0 y_d(t), \quad (24)$$

with coefficients $p_0, \ldots, p_n$ computed upon (22)-(23) will be called the *corrected-approximate-inverse* (CAI) controller. The name reflects the fact that design equation (23) corrects a simplistic inverse of (1), resulting only from the inverse of denominator polynomial $A(s)$, by the values of coefficients of numerator polynomial $B(s)$.

Next, let the degree of polynomial $P(s)$ extend over the order of plant dynamics, i.e. $\mu > n$. In this case, it is possible to further reduce the mismatch transfer function (21) by zeroing subsequent coefficients $w_{n+1}, \ldots, w_\mu$ of polynomial $\breve{W}(s)$, see (17). Following this design guideline, and recalling

[1] In contrast to the case of discrete-time systems, where smoothness of a reference trajectory is usually not an issue thanks to the specific form of discrete-time controllers operating only on samples of appropriate signals (a reader interested in discrete-time feedforward controllers is referred e.g. to [4], [21] and references cited therein).

(20) under assumption A2, one obtains the recursive design equation of extending coefficients (note: $a_j = 0$ for $j > n$)

$$p_j \triangleq -\sum_{i=1}^{j} b_i p_{j-i} \quad \text{for} \quad j \in \{n+1, \ldots, \mu\}. \tag{25}$$

Now, the following *extended-approximate-inverse* (EAI) controller can be defined for $\mu > n$:

$$u_{\text{FF}}^{\text{EAI}}(t) \triangleq p_\mu y_d^{(\mu)}(t) + \ldots + p_{n+1} y_d^{(n+1)}(t) + u_{\text{FF}}^{\text{CAI}}(t), \tag{26}$$

where $u_{\text{FF}}^{\text{CAI}}(t)$ results from definition (24).

Application of the CAI/EAI (in short: XAI) controllers allows reducing the mismatch function (21) to the form

$$\begin{aligned} \Gamma^{\text{XAI}}(s) &= 1 - G(s) G_{\text{FF}}^{\text{XAI}}(s) \\ &\overset{(17)}{=} \frac{w_{\mu+m} s^{\mu+m} + \ldots + w_{\mu+1} s^{\mu+1}}{A(s)}, \end{aligned} \tag{27}$$

where $\mu = n$ for CAI and $\mu > n$ for EAI controller. The form of mismatch transfer function $\Gamma^{\text{XAI}}(s)$ determines the best possible tracking performance attainable in the closed-loop system with a fixed stabilizing controller G_R and with CAI or EAI feedforward applied (see Section IV-A).

Remark 3: Although in the paper we are focused on the plant-inversion feedforward, the proposed XAI controllers can be employed also in a system with the closed-loop-inversion feedforward illustrated in Fig. 2. In this case, the transfer

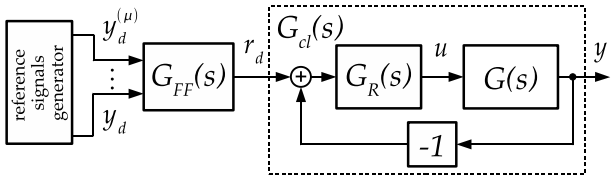

Fig. 2. The 2DOF control system with the closed-loop-inversion feedforward.

function $G_{\text{FF}}(s)$ is designed as an (approximate) inverse of the closed-loop dynamics represented by transfer function $G_{cl}(s) \triangleq Y(s)/R_d(s)$. In particular, if

$$G_{cl}(s) = \frac{G_R(s)G(s)}{1 + G_R(s)G(s)} = \frac{L(s)B(s)}{M(s)A(s) + L(s)B(s)} = \frac{\bar{B}(s)}{\bar{A}(s)}$$

will be treated as a ratio of some resultant polynomials $\bar{B}(s) = \bar{b}_m s^m + \ldots + \bar{b}_1 s + \bar{b}_0$ and $\bar{A}(s) = \bar{a}_n s^n + \ldots + \bar{a}_1 s + \bar{a}_0$ satisfying assumptions A1 and A2, then the error transfer function for the system from Fig. 2 results from the equation

$$G_E(s) \triangleq \frac{E(s)}{Y_d(s)} = 1 - G_{cl}(s) G_{\text{FF}}(s) =: \Gamma_{cl}(s), \tag{28}$$

where $E(s) = Y_d(s) - Y(s)$ represents the tracking error, while $\Gamma_{cl}(s)$ denotes a feedforward mismatch function for the closed-loop-inversion approach. According to (28), a tracking accuracy depends in this case only on the mismatch function, which for the fixed-structure feedforward (11) takes the form

$$\Gamma_{cl}(s) = 1 - \frac{\bar{B}(s)}{\bar{A}(s)} P(s) = \frac{\bar{A}(s) - \bar{B}(s)P(s)}{\bar{A}(s)} = \frac{\bar{W}(s)}{\bar{A}(s)}. \tag{29}$$

Since the structure of mismatch function (29) is analogous to (21), the key reasoning presented in Sections III-A and III-B applies also here. As a consequence, XAI feedforward controllers for the closed-loop-inversion case can be synthesized upon the same equations (22)-(26) but now using coefficients $\bar{b}_i$ and $\bar{a}_j$ taken from the resultant polynomials $\bar{B}(s)$ and $\bar{A}(s)$, respectively. Worth to emphasize that transfer function (28) directly depends on a structure and parameters of the controller transfer function $G_R(s)$. Therefore, in contrast to the plant-inversion feedforward case, designing the closed-loop-inversion feedforward is dependent on feedback controller dynamics.

Remark 4: Since practical implementations of today control systems are mostly on digital devices, a justified question arises about discrete-time versions of XAI controllers. This issue involves distinguishing between two alternative approaches to the discrete-time (DT) control synthesis problem. Let us shortly comment this issue with a help of a chart presented in Fig. 3. The proposed feedforward control law (3) has been determined in the continuous-time (CT) domain as a *nominal* choice for the case where dynamics of a plant is described by the CT model (the nominal CT-CT case highlighted in gray in Fig. 3). Designing the DT version of the controller for the CT

controller \ plant	CT	DT
CT	nominal case	---
DT	approximate case	nominal case

Fig. 3. A chart collecting possible combinations of continuous-time (CT) or discrete-time (DT) controller applied to a plant described in the continuous-time (CT) or discrete-time (DT) domain; the nominal case considered in the paper is highlighted in gray.

plant dynamics shall be treated as an approximate approach which can be addressed generally in two alternative ways: by discretization of a controller structure originally designed in the CT domain, or by DT approximation of the CT plant dynamics followed by a design of a DT controller. Both approaches lead to very similar control performance when sampling time $T_s > 0$ used for discretization is sufficiently small relative to a bandwidth of plant dynamics. The former approach, however, seems simpler by preserving very intuitive controller synthesis performed in the CT domain. Assuming this line of reasoning, a DT version of XAI control law is especially simple and results only from sampling of the reference trajectory and its time-derivatives with sampling time T_s, that is

$$u_{\text{FF}}^{\text{XAI}}(kT_s) \triangleq p_\mu y_d^{(\mu)}(kT_s) + \ldots + p_1 y_d^{(1)}(kT_s) + p_0 y_d(kT_s), \tag{30}$$

where $k = 0, 1, 2 \ldots$ Worth to stress that all the signals used on the right-hand side of the above equation are available at any time instant $t = kT_s$ upon assumption A4. Efficiency of XAI controllers in the DT version (30) can be assessed upon exemplary experimental results presented in Section V-B where the DT feedforward was applied to the CT plant with sampling time $T_s = 0.01\,\text{s}$. Designing the DT versions of XAI feedforward controllers directly for DT plants involves separate investigations and is out of the paper scope.

IV. Analysis of approximate-inverse controllers

A. Properties of XAI controllers

Let us analyze how XAI controllers affect tracking error (2). According to (13), one can write the frequency-domain relation

$$E(\bar{j}\omega) = S(\bar{j}\omega)\Gamma(\bar{j}\omega)Y_d(\bar{j}\omega), \tag{31}$$

where the product $S(\bar{j}\omega)\Gamma(\bar{j}\omega)$ can be treated as a frequency-weighted sensitivity function with weight $\Gamma(\bar{j}\omega)$. Since $S(\bar{j}\omega)$, for a given plant dynamics $G(s)$, is determined solely by a stabilizing controller, a feedforward controller is responsible for decreasing $|\Gamma(\bar{j}\omega)|$ as much as possible to obtain an acceptable tracking accuracy at least over some finite frequency range of interest. Hereafter, we will particularly consider a low-frequency range

$$\Omega \triangleq [0, \omega_g], \quad 0 < \omega_g < \infty \tag{32}$$

where ω_g determines a frequency band for a reference trajectory, that is, a frequency range beyond which an amplitude spectrum of $y_d(t)$ is zero or can be neglected. Selection of range (32) has been motivated by the fact that most practical plants exhibit low-pass dynamics.

We are going to analyze properties of the mismatch function for CAI and EAI feedforward controllers, especially over the frequency range defined by (32). For simplicity, we will refer to the XAI mismatch function (27), which boils down to the CAI case by taking $\mu = n$.

By rewriting (27) in the form

$$\Gamma^{\text{XAI}}(s) = \frac{(w_{\mu+m}s^{m-1} + \ldots + w_{\mu+1})s^{\mu+1}}{A(s)} = \frac{\breve{W}^*(s)s^{\mu+1}}{A(s)}$$

one can easily find that the logarithmic module

$$\begin{aligned}\text{Lm}^{\text{XAI}}(\omega) &\triangleq 20\log\left|\Gamma^{\text{XAI}}(\bar{j}\omega)\right| \\ &= 20(\mu+1)\log\omega + 20\log\left|\breve{W}^*(\bar{j}\omega)\right| - 20\log|A(\bar{j}\omega)|\end{aligned}$$

can be approximated in a low frequency range (i.e. for sufficiently small $\omega \in \Omega$) by

$$\text{Lm}^{\text{XAI}}(\omega) \approx 20(\mu - i + 1)\log\omega + \chi^{\text{XAI}}, \tag{33}$$

where $\chi^{\text{XAI}} = 20\log|w_{\mu+1}| - 20\log|a_i|$, while i is the index of a non-zero coefficient a_i corresponding to the least power of s in polynomial $A(s)$. Thus, for any $\mu \geq n$ the following convergence is satisfied:

$$\text{Lm}^{\text{XAI}}(\omega \to 0) \to -\infty \quad \Rightarrow \quad \left|\Gamma^{\text{XAI}}(\bar{j}\omega \to 0)\right| \to 0.$$

In a low frequency range, the rate of convergence is monotonic with approximately constant slope

$$N^{\text{XAI}}(\omega) \triangleq \frac{d\,\text{Lm}^{\text{XAI}}(\omega)}{d\log\omega} \approx 20(\mu - i + 1)\,\text{dB/dec}. \tag{34}$$

It means that the XAI feedforward controllers guarantee improvement of tracking performance for the reference trajectories y_d having the amplitude spectra contained in a sufficiently narrow range Ω.

Further, according to (33), the low-frequency slopes of functions $\text{Lm}^{\text{EAI}}(\omega)$ and $\text{Lm}^{\text{CAI}}(\omega)$ depend on degree μ of feedforward polynomial (11), and they are equal, respectively, to $20(\mu - i + 1)$ dB/dec and $20(n - i + 1)$ dB/dec. Thus, for $\mu > n$ the function $\text{Lm}^{\text{EAI}}(\omega)$ either lies entirely under $\text{Lm}^{\text{CAI}}(\omega)$ over the range Ω, or it intersects function $\text{Lm}^{\text{CAI}}(\omega)$ at some frequency $\omega_c^{\text{XAI}} \approx |w_{n+1}/w_{\mu+1}|^{1/(\mu-n)}$, which has been estimated upon equation (33). As a consequence, one may conclude that

$$\exists\,\Omega^* = [0, \omega^*) : \ \forall\,\omega \in \Omega^* \ \left|\Gamma^{\text{EAI}}(\bar{j}\omega)\right| < \left|\Gamma^{\text{CAI}}(\bar{j}\omega)\right|, \tag{35}$$

where $\omega^* = \min\{\omega_c^{\text{XAI}}, \omega_g\}$, that is, the EAI controller outperforms the CAI controller over the range Ω^*. The difference between logarithmic modules

$$\begin{aligned}\Delta\text{Lm}(\omega) &\triangleq \text{Lm}^{\text{EAI}}(\omega) - \text{Lm}^{\text{CAI}}(\omega) \\ &\approx 20(\mu - n)\log\omega + 20\log|w_{\mu+1}/w_{n+1}|\end{aligned}$$

increases proportionally to the difference $\mu - n$ at any fixed frequency $\omega \in \Omega^*$. One may conclude, that successive increasing of μ above degree n ensures gradual improvement of tracking control performance at any $\omega \in \Omega^*$.

Worth considering yet another interpretation of equation (31). Let $Z_d(\bar{j}\omega) \triangleq \Gamma(\bar{j}\omega)Y_d(\bar{j}\omega)$ represent a Fourier transform of a fictitious input signal to the closed-loop system, which in the time domain for XAI feedforward controllers can be described as

$$z_d(t) \overset{(27)}{=} \frac{1}{A(s)}\left[w_{\mu+m}y_d^{(\mu+m)}(t) + \ldots + w_{\mu+1}y_d^{(\mu+1)}(t)\right].$$

The above equation may be interpreted as a low-pass filtered (through filter $F(s) = 1/A(s)$) weighted combination of the higher-order time-derivatives of reference trajectory $y_d(t)$. Thus, in a special case of a reference trajectory for which the higher-order time-derivatives vanish with order, and when $A(s)$ is Hurwitz, the error peak

$$\operatorname*{ess\,sup}_{t\geq 0}|e(t)| \leq \epsilon_s\epsilon_f \cdot \sum_{i=\mu+1}^{\mu+m}|w_i| \sup_{t\geq 0}\left|y_d^{(i)}(t)\right|,$$

with $\epsilon_s = \int_0^\infty \left|\mathcal{L}^{-1}\{S(s)\}(t)\right| dt < \infty$ and $\epsilon_f = \int_0^\infty \left|\mathcal{L}^{-1}\{1/A(s)\}(t)\right| dt < \infty$, can be made sufficiently small by increasing μ (note: $\epsilon_s < \infty$ upon assumption A3, while $\epsilon_f < \infty$ if $A(s)$ is Hurwitz).

Remark 5: Worth recalling that the 2-norm of the transient error $e(t)$ cannot be made arbitrarily small when a plant has the nonminimum-phase dynamics. It is a fundamental limitation addressed by various investigators (see e.g. [1], [18], [22]), which is independent of a control method applied.

Remark 6: Application of EAI controller seems to be unjustifiable when the plant transfer function has a time-delay term approximated by its finite Taylor-series expansion (8) or (10), see Remark 1. These kinds of approximation influence the order of dynamics (1). Thus, extension of degree μ in (11) shall follow prior inclusion of the next higher-order terms from the Taylor-series expansion to make the approximation more accurate, which leads again to the CAI control law but with higher degree μ. The above intuition has been verified by simulation example in Section V-A.

Remark 7: In a special case, when the plant transfer function have no zeros and no time-delay, then $B(s) = D(s) = 1$,

$A(s) = C(s)$ (cf. (1) and (7)), and feedforward coefficients $p_j = c_j = a_j$ for $j = 0, \ldots, n$ (see (22)-(23)). As a consequence, the CAI control law (24) corresponds to the classical model-inverse feedforward $G_{\rm FF}(s) = G^{-1}(s)$ which guarantees perfect (asymptotic) tracking in the closed-loop system.

B. Comparison of XAI controllers with classical methods

We are going to qualitatively compare effectiveness of the newly proposed control law with three classical approximate-inverse feedforward methods – NZI, ZME, and ZPE – for the particular case where a plant has the nonminimum-phase dynamics ($B^p(s) \not\equiv 1$). To this aim, let us recall transfer functions of the classical controllers and their special forms obtained under assumption A2:

$$G_{\rm FF}^{\rm NZI}(s) \triangleq \frac{A(s)}{B^n(s)B^p(0)} = \frac{A(s)}{B^n(s)}, \tag{36}$$

$$G_{\rm FF}^{\rm ZME}(s) \triangleq \frac{A(s)}{B^n(s)B^p(-s)}, \tag{37}$$

$$G_{\rm FF}^{\rm ZPE}(s) \triangleq \frac{A(s)B^p(-s)}{B^n(s)[B^p(0)]^2} = \frac{A(s)B^p(-s)}{B^n(s)}. \tag{38}$$

Recalling definition of the mismatch function (13), the form of polynomial (5), and plant dynamics (1) one gets

$$\Gamma^{\rm NZI}(s) \overset{(36)}{=} 1 - B^p(s) = -\beta_\gamma s^\gamma - \ldots - \beta_1 s,$$

$$\Gamma^{\rm ZME}(s) \overset{(37)}{=} 1 - \frac{B^p(s)}{B^p(-s)} = \frac{[(-1)^\gamma - 1]\beta_\gamma s^\gamma - \ldots - 2\beta_1 s}{(-1)^\gamma \beta_\gamma s^\gamma + \ldots - \beta_1 s + 1},$$

$$\Gamma^{\rm ZPE}(s) \overset{(38)}{=} 1 - B^p(s)B^p(-s) = -\bar\beta_{2\gamma} s^{2\gamma} - \ldots - \bar\beta_2 s^2,$$

where the numerator of $\Gamma^{\rm ZME}(s)$ includes only terms with odd powers of s, while polynomial of $\Gamma^{\rm ZPE}(s)$ comprises only terms with even powers of s.

Continuing reasoning from Section IV-A, let us estimate slopes of the logarithmic module functions ${\rm Lm}^{\rm NZI}(\omega)$, ${\rm Lm}^{\rm ZME}(\omega)$, and ${\rm Lm}^{\rm ZPE}(\omega)$. Upon the forms of the above mismatch transfer functions one may (conservatively) assess upper bounds of particular slopes for sufficiently low frequencies $\omega \in \Omega$ as follows:

$$N^{\rm NZI}(\omega) \lessapprox 20\gamma \le 20m \le 20n \,{\rm dB/dec}, \tag{39}$$

$$N^{\rm ZME}(\omega) \lessapprox 20\gamma \le 20m \le 20n \,{\rm dB/dec}, \tag{40}$$

$$N^{\rm ZPE}(\omega) \lessapprox 20 \cdot 2\gamma \,{\rm dB/dec}, \tag{41}$$

where estimation in (39)-(40) comes from the fact that $\gamma \le m \le n$ according to assumptions A1 and A2. Comparing (34) with estimates (39)-(41) one can conclude that for sufficiently low $\omega \in \Omega$ hold:

$$\left.\begin{array}{l} N^{\rm XAI}(\omega) > N^{\rm NZI}(\omega) \\ N^{\rm XAI}(\omega) > N^{\rm ZME}(\omega) \end{array}\right\} \quad \text{for} \quad \mu > \gamma + i - 1, \tag{42}$$

$$N^{\rm XAI}(\omega) > N^{\rm ZPE}(\omega) \qquad \text{for} \quad \mu > 2\gamma + i - 1. \tag{43}$$

Thus, there exists sufficiently large $\mu \ge n$ satisfying (42) and (43) such that ${\rm Lm}^{\rm XAI}(\omega)$ either lies entirely under functions ${\rm Lm}^{\rm NZI}(\omega)$, ${\rm Lm}^{\rm ZME}(\omega)$, and ${\rm Lm}^{\rm ZPE}(\omega)$ over the range Ω, or it intersects functions ${\rm Lm}^{\rm NZI}(\omega)$, ${\rm Lm}^{\rm ZME}(\omega)$, and ${\rm Lm}^{\rm ZPE}(\omega)$ at some frequencies $\omega_c^{\rm NZI}$, $\omega_c^{\rm ZME}$, and $\omega_c^{\rm ZPE}$, respectively. As a consequence, one concludes that for sufficiently large $\mu \ge n$

$$\exists\, \tilde\Omega = [0, \tilde\omega) : \ \forall\, \omega \in \tilde\Omega \quad \left|\Gamma^{\rm XAI}(\bar\jmath\omega)\right| < \left|\Gamma^{\rm YYY}(\bar\jmath\omega)\right|, \tag{44}$$

where $\tilde\omega = \min\{\omega_c^{\rm NZI}, \omega_c^{\rm ZME}, \omega_c^{\rm ZPE}, \omega_g\}$, and ${\rm YYY} \in \{{\rm NZI}, {\rm ZME}, {\rm ZPE}\}$. It means that for sufficiently large μ the XAI controllers improve tracking control performance over the range $\tilde\Omega \subseteq \Omega$ relative to all three classical approximate-inverse feedforward methods when a plant has the nonminimum-phase dynamics.

Thanks to the form of error transfer function (28), the above reasoning can be repeated for the mismatch function $\Gamma_{cl}(\bar\jmath\omega)$ leading to analogous general conclusions for the case of the closed-loop-inversion feedforward when a closed-loop system has the nonminimum-phase dynamics.

Remark 8: Assessments of degree μ in (42) and (43) are conservative, since they result from the *cautious* estimation made in (33) together with the *worst-case* assumption where the mismatch functions $\Gamma^{\rm NZI}(s)$, $\Gamma^{\rm ZME}(s)$, and $\Gamma^{\rm ZPE}(s)$ reduce to single terms of their numerators corresponding to the highest power of s. Thus in particular cases, the left-hand side inequalities of (42)-(43) can be satisfied for lower degree μ than estimated in (42)-(43).

Remark 9: If the plant transfer function (1) has zeros solely in the left-half complex plane (the minimum-phase plant with $B(s) \equiv B^n(s) \not\equiv 1$) then the XAI controllers give only an approximate feedforward, even so the accurate feedforward $G_{\rm FF}^{\rm NZI} = G_{\rm FF}^{\rm ZME} = G_{\rm FF}^{\rm ZPE} = A(s)/B^n(s)$ exists and could be applied in this case. This limitation of the proposed method seems to have rather moderate consequences in practical applications because one can make approximate feedforward (3) arbitrarily close to the accurate one in a low frequency range by increasing the degree μ. On the other hand, the process of successive increasing of μ will finally reach a practical limitation once a tracking error level reaches a level of a measurement noise present in a feedback signal (any further potential improvement of a tracking accuracy resulting from continued increasing of μ will be lost by immersion in the noise – see Section V-B).

V. Verification of the Method

A. Numerical examples

Four numerical examples, denoted as SimA, SimB, SimC, and SimD, illustrate main properties of the proposed feedforward controllers. During simulations, three controllers have been applied: CAI, EAI1, and EAI2, where the latter two denote the extended approximate-inverse feedforward with the one-order ($\mu = n + 1$) and two-order ($\mu = n + 2$) extension, respectively. The feedforward controllers have been applied in the closed-loop system from Fig. 1 with proportional stabilizer $G_R = k_p$ with $k_p = 1.6$ for SimA, $k_p = 1.0$ for SimB and SimC, and $k_p = 0.2$ for SimD. Simulation results illustrate control performance in a response to reference trajectory $y_d(t) \triangleq 0.5\sin(0.4t) + 1.0\sin(0.2t) + 1.5\sin(0.1t)$, employing the following switching pattern for feedforward control: no feedforward for $t \in [0, 100)$ s, CAI for $t \in [100, 200)$ s,

EAI1 for $t \in [200, 300)$ s, and EAI2 for $t \in [300, 400]$ s (with exception of example SimC$_3$ where CAI controller has been only switched to EAI1 feedforward at $t = 200$ s). The following exemplary plant dynamics have been selected for SimA, SimB, SimC, and SimD, respectively:

$$G_A = \frac{-0.4s+1}{0.3s^2+0.8s-1.5}, \quad \begin{matrix} z_1 = +2.50 \\ s_1 = +1.27, s_2 = -3.94 \end{matrix}$$

$$G_B = \frac{-s^2+1}{0.25s^3+1.75s^2+4s+3}, \quad \begin{matrix} z_1 = +1.0, z_2 = -1.0 \\ s_1 = -3.0, s_{2,3} = -2.0 \end{matrix}$$

$$G_C = \frac{-0.2s+1}{s+2}\exp(-s), \quad \begin{matrix} z_1 = +5.0 \\ s_1 = -2.0 \end{matrix}$$

$$G_D = \frac{-0.1s+1}{s^2+s}, \quad \begin{matrix} z_1 = +10.0 \\ s_1 = 0.0, s_2 = -1.0 \end{matrix}$$

where zeros z_i and poles s_i of the particular transfer functions have been denoted on the right-hand side. Transfer function G_C was approximated by two rational dynamics (corresponding to simulation cases denoted by SimC$_2$ and SimC$_3$, respectively)

$$G_{C2} \overset{(8)}{=} \frac{-0.2s+1}{0.5s^3+2s^2+3s+2},$$
$$G_{C3} \overset{(8)}{=} \frac{-0.2s+1}{0.17s^4+0.83s^3+2s^2+3s+2},$$

obtained by using expansion (8) for $\nu = 2$ and $\nu = 3$, respectively. Values of coefficients p_j, $j = 0, \ldots, \mu$, computed for particular simulation examples are collected in Table I (coefficients used for CAI control law are denoted in bold). The results of numerical simulations are presented in Figs. 4-8.

TABLE I
COMPUTED COEFFICIENTS OF CAI/EAI CONTROLLERS

coefficient	SimA	SimB	SimC$_2$	SimC$_3$	SimD
p_0	$\mathbf{-1.500}$	$\mathbf{3.000}$	$\mathbf{2.000}$	$\mathbf{2.000}$	$\mathbf{0.000}$
p_1	$\mathbf{0.200}$	$\mathbf{4.000}$	$\mathbf{3.400}$	$\mathbf{3.400}$	$\mathbf{1.000}$
p_2	$\mathbf{0.380}$	$\mathbf{4.750}$	$\mathbf{2.680}$	$\mathbf{2.680}$	$\mathbf{1.100}$
p_3	0.152	$\mathbf{4.250}$	$\mathbf{1.036}$	$\mathbf{1.369}$	0.110
p_4	0.061	4.750	0.207	$\mathbf{0.441}$	0.011
p_5	–	4.250	0.041	0.088	–

In example SimA, the plant is represented by the second-order unstable transfer function G_A which has a single positive zero. Figure 4 shows substantial tracking improvement after turning CAI feedforward on at $t = 100$ s, and then successive improvements of tracking accuracy after switching to EAI1 and EAI2 controllers. Further increasing of μ will provide continued reduction of the tracking error bound. The Bode-magnitude plot of error transfer function (12) in Fig. 4 indicates that all XAI controllers shall improve tracking performance for the considered reference trajectory when compared to the classical feedforward laws. It is confirmed by the comparative plot of absolute tracking errors on the right-hand side in Fig. 4 obtained for NZI, ZME, ZPE and three considered XAI controllers (note: in this case $\gamma = 1$ and $i = 0$, thus (42) and (43) are met by all XAI controllers). A tracking accuracy improvement achieved with EAI2 controller relative to ZPE feedforward amounts in this case about two orders of magnitude for tracking error bounds.

Similar conclusions can be formulated upon the plots presented in Fig. 5 for the example SimB. In this case, the third-order plant G_B is stable but has one positive and one negative zero which dominate the poles. Tracking improvement achieved with EAI2 controller relative to ZPE feedforward amounts more than one order of magnitude for tracking error bounds.

Plots in Fig. 6 obtained for the nonminimum-phase delay-dominated plant G_C confirm the intuition formulated in Remark 6, according to which application of EAI controllers does not improve tracking performance relative to the CAI one. In this context, worth noting the Bode-magnitude plot shown in Fig. 6 where the characteristics of $|G_E(\bar{j}\omega)|$ almost overlap in the low-frequency range for all the CAI and EAI controllers. However, by including in G_{C3} the higher-order terms of Taylor-series expansion (8), the feedforward polynomial degree μ has been naturally increased, and the new form of CAI controller obtained in this way has become more effective as can be seen in Fig. 7 (when compared with Fig. 6). Similarly as before, application of EAI controller does not improve tracking performance more (indicated also by the Bode-magnitude plot[2]), however, one can see substantial tracking improvement obtained in this case with CAI controller relative to the classical ones.

Example SimD illustrates the results for the nonminimum-phase marginally stable plant dynamics with a single pole equal to zero. In this case, the EAI1 and EAI2 feedforward controllers gradually improve tracking performance relative to CAI controller. However, when compared to the classical feedforward control laws (see the comparative tracking-errors plot on the right-hand side in Fig. 8), one can see that application of CAI feedforward leads to worse tracking performance than the one obtained with classical ZPE control law. It is a direct consequence of condition (43), upon which the tracking control improvement with XAI feedforward is guaranteed for $\mu > 2$ (note: in this case $\gamma = 1$ and $i = 1$). Since $\mu = n = 2$ for CAI controller, a tracking accuracy improvement over ZPE method can be obtained by applying EAI controller with $\mu > n = 2$. Nearly two orders of magnitude improvement can be seen in Fig. 8 for tracking error bounds obtained with EAI2 controller.

Summarizing the comments to simulation results, worth to note that a quantitative tracking accuracy improvement achievable due to application of XAI controllers depends on relative locations of poles and zeros of the approximated plant dynamics. Similar effect was observed and studied for the classical feedforward methods, see e.g. [3], [4]. Further, one shall also mention that tracking accuracy improvement in a low frequency range by application of XAI controllers has a consequence in the form of tracking performance degradation in a high-frequency range. This waterbed-like effect, (generally common to the XAI and classical controllers), can be observed in the Bode-magnitude plots in Figs. 4-8, where one can observe substantial increase of the error transfer function module at high frequencies with increase of degree μ. Practical

[2]The error transfer function (12) has been computed for the example SimC by taking $G = G_C$ with the time delay term approximated by the 5-order Padé method (function `PADE(1,5)` in Matlab).

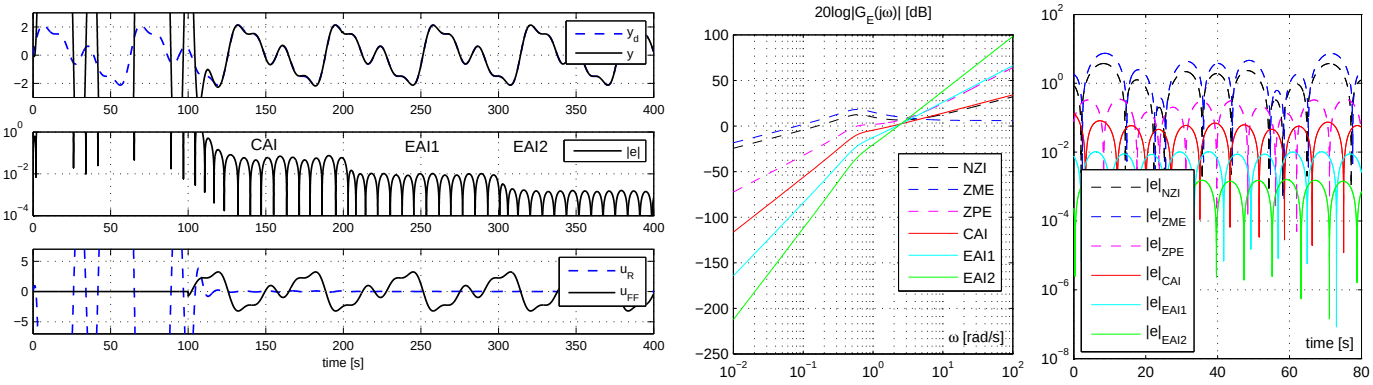

Fig. 4. SimA: Time-plots of selected signals (left), Bode-magnitude plot of error transfer function (12) for the classical and proposed feedforward controllers (middle), and comparison of absolute tracking errors in a logarithmic scale obtained with various feedforward control laws in the case of plant G_A (right).

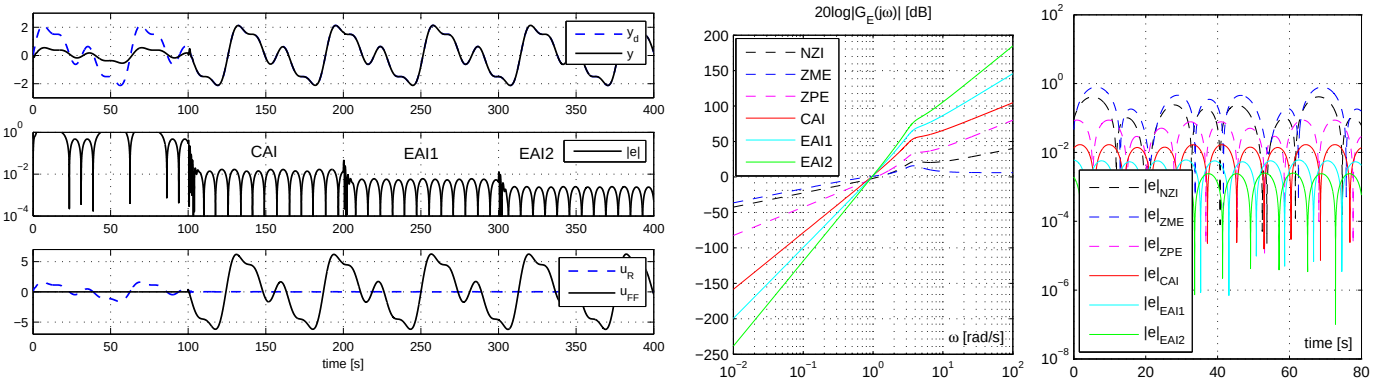

Fig. 5. SimB: Time-plots of selected signals (left), Bode-magnitude plot of error transfer function (12) for the classical and proposed feedforward controllers (middle), and comparison of absolute tracking errors in a logarithmic scale obtained with various feedforward control laws in the case of plant G_B (right).

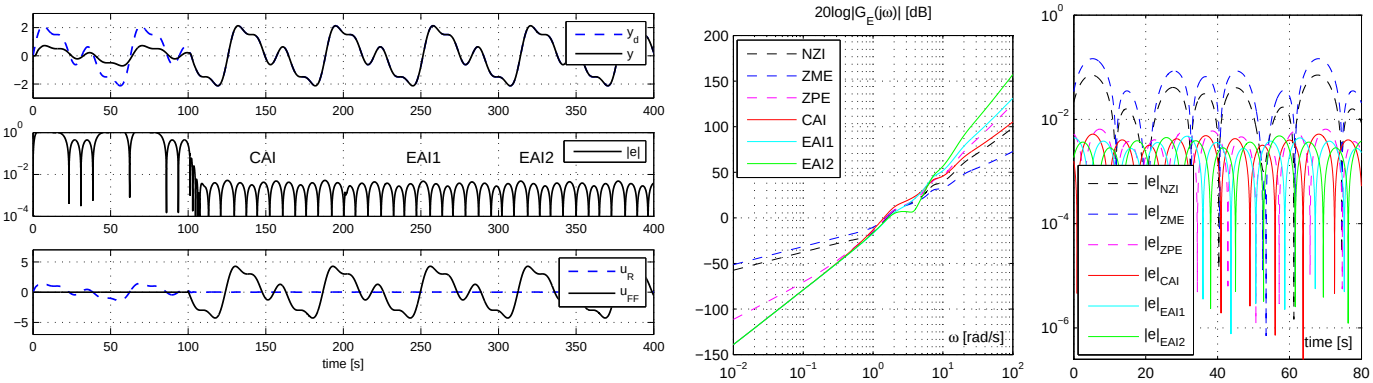

Fig. 6. SimC$_2$: Time-plots of selected signals (left), Bode-magnitude plot of error transfer function (12) for the classical and proposed feedforward controllers (middle), and comparison of absolute tracking errors in a logarithmic scale obtained with various feedforward control laws in the case of plant G_C approximated by G_{C2} (right).

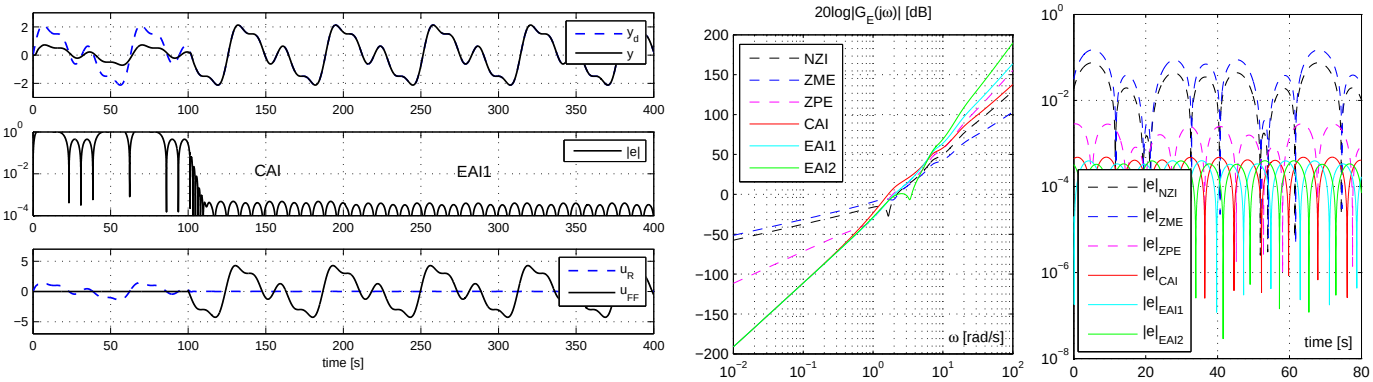

Fig. 7. SimC$_3$: Time-plots of selected signals (left), Bode-magnitude plot of error transfer function (12) for the classical and proposed feedforward controllers (middle), and comparison of absolute tracking errors in a logarithmic scale obtained with various feedforward control laws in the case of plant G_C approximated by G_{C3} (right).

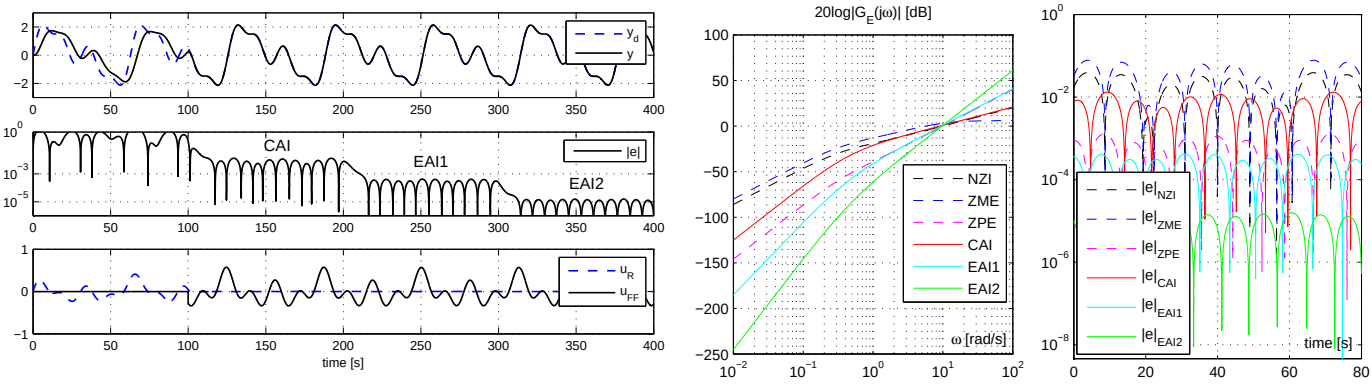

Fig. 8. SimD: Time-plots of selected signals (left), Bode-magnitude plot of error transfer function (12) for the classical and proposed feedforward controllers (middle), and comparison of absolute tracking errors in a logarithmic scale obtained with various feedforward control laws in the case of plant G_D (right).

consequences of this effect shall be taken into account when a reference signal contains high-frequency components.

Remark 10: To make a view more comprehensive, the two exemplary Bode-magnitude plots of error transfer function (28) have been presented in Fig. 9 in the case of the closed-loop-inversion feedforward (cf. Fig. 2) designed for plants represented by transfer functions G_A and G_B. One can see similar

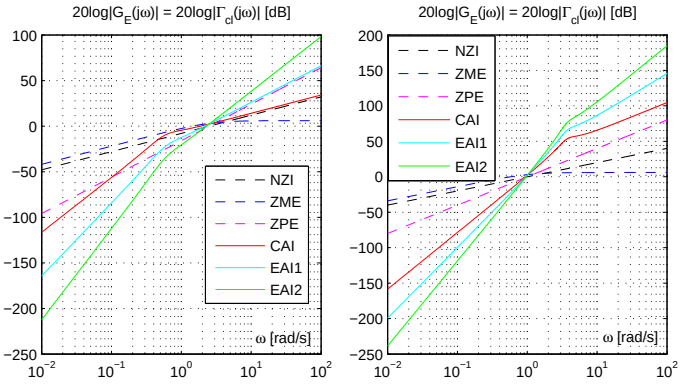

Fig. 9. Bode-magnitude plots of error transfer function (28) for the classical and proposed XAI controllers in two cases of the plant transfer function: G_A (left) and G_B (right).

tendency as in the plant-inversion feedforward case, where XAI controllers ensure gradual tracking control improvement in a low frequency range by increasing of degree μ. Worth noting, however, less beneficial result (in the quantitative sense) obtained here for plant G_A relative to the result presented in Fig. 4 where the plant-inversion feedforward was applied.

B. Experimental validation

The proposed feedforward controllers have been validated experimentally to show their effectiveness in the presence of a model parametric uncertainty and a measurement noise. The plant *HILSys* used for experiments was an analog electronic circuit with operational amplifiers build in the MAX 265 chip equipped with external adjustable resistive potentiometers. The control input voltage u and plant output y have been applied/measured in a quasi real time in a fast-prototyping system comprising the I/O card PCI-DAS1602/12 and a PC computer with the VisSim+RealTimePRO software (see Fig. 10).

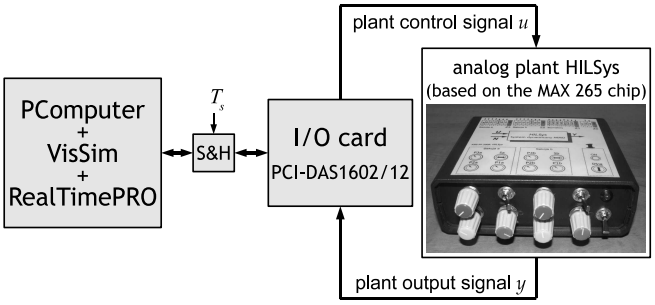

Fig. 10. Experimental testbed scheme with analog electronic plant HILSys.

Input-output signals were sampled with a constant sampling interval $T_s = 0.01\,\mathrm{s}$. A plant model has been estimated using the SVF-RLS method, [10], yielding the second-order transfer function $\hat{G}(s) \triangleq \hat{Y}(s)/U(s)$, where

$$\hat{G}(s) = \frac{\hat{b}_1 s + 1}{\hat{a}_2 s^2 + \hat{a}_1 s + \hat{a}_0} = \frac{-0.1864s + 1}{0.0354s^2 + 0.0809s + 1.0042}$$

has a single positive zero $z_1 = +5.3648$ and a pair of complex poles $s_{1,2} = -1.1427 \pm 5.2021\bar{j}$. A step response of model $\hat{G}(s)$ is presented in Fig. 11.

Validation has been performed for CAI and two versions of EAI controllers, denoted as EAI1 and EAI2, the latter ones designed for the first order ($\mu = 3$) and second order ($\mu = 4$) extension, respectively. Particular feedforward controllers take

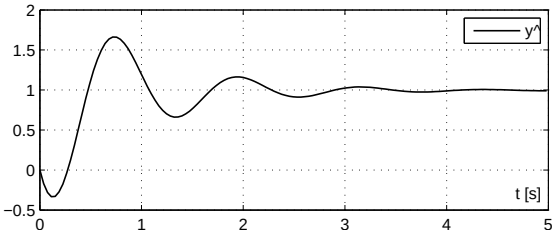

Fig. 11. A step response of nonminimum-phase transfer function $\hat{G}(s)$.

the forms

$$u_{\mathrm{FF}}^{\mathrm{CAI}} = p_2 y_d^{(2)} + p_1 y_d^{(1)} + p_0 y_d,$$
$$u_{\mathrm{FF}}^{\mathrm{EAI1}} = p_3 y_d^{(3)} + p_2 y_d^{(2)} + p_1 y_d^{(1)} + p_0 y_d,$$
$$u_{\mathrm{FF}}^{\mathrm{EAI2}} = p_4 y_d^{(4)} + p_3 y_d^{(3)} + p_2 y_d^{(2)} + p_1 y_d^{(1)} + p_0 y_d$$

with the following values of weighting coefficients: $p_0 = 1.0042$, $p_1 = 0.2681$, $p_2 = 0.0854$, $p_3 = 0.0159$, and $p_4 = 0.0030$. XAI controllers were implemented in the fast-prototyping system using their DT versions represented by (30) for $T_s = 0.01\,\mathrm{s}$. Two separate tests have been performed in a closed-loop system with proportional stabilizing controller $G_R \triangleq k_p = 0.1$ in a response to reference signal $y_d(t) \triangleq \sin(\omega_d t)$ applied for two values of reference frequency $\omega_d \in \{1.0, 2.0\}\,\mathrm{rad/s}$. In both tests, the stabilizing controller worked alone for the first ten seconds, and then a selected feedforward controller was turned on. The results of tracking performance are presented in Fig. 12. They have been compared with tracking errors obtained for three classical feedforward controllers, which for plant $\hat{G}(s)$ take the forms[3]:

$$u_{\mathrm{FF}}^{\mathrm{NZI}} = \hat{a}_2 y_d^{(2)} + \hat{a}_1 y_d^{(1)} + \hat{a}_0 y_d,$$
$$u_{\mathrm{FF}}^{\mathrm{ZME}} = \frac{1}{-\hat{b}_1 s + 1}\left[\hat{a}_2 y_d^{(2)} + \hat{a}_1 y_d^{(1)} + \hat{a}_0 y_d\right],$$
$$u_{\mathrm{FF}}^{\mathrm{ZPE}} = -\hat{b}_1\hat{a}_2 y_d^{(3)} + (\hat{a}_2 - \hat{b}_1\hat{a}_1) y_d^{(2)} + (\hat{a}_1 - \hat{b}_1\hat{a}_0) y_d^{(1)} + \hat{a}_0 y_d.$$

For the purpose of quantitative comparison of the methods, the performance index $J_e \triangleq \int_{t_1}^{t_2} e^2(t)dt$ has been computed for the last thirty seconds of the experiments. Values of the index obtained during the tests are collected in Table II. The last two

TABLE II
VALUES OF PERFORMANCE INDEX J_e FOR VARIOUS FEEDFORWARD CONTROLLERS AND SINUSOIDAL REFERENCE SIGNAL $y_d = \sin(\omega_d t)$

Method	J_e for $\omega_d = 1\,\mathrm{rad/s}$	J_e for $\omega_d = 2\,\mathrm{rad/s}$
NZI	0.4745	1.9872
ZME	1.8130	6.5812
ZPE	0.0214	0.3445
CAI	0.0046	0.2424
EAI1	0.0034*	0.0231
EAI2	0.0051*	0.0159*

plots of every column in Fig. 12 present amplitude spectra of (sampled) tracking-error signals computed for particular control methods with sampling interval $T_s = 0.01\,\mathrm{s}$ according to definition:

$$|E_N(\omega_k)| \triangleq \frac{2}{N}\sum_{k=0}^{N-1} e(kT_s)\exp(-\bar{j}kT_s\omega_k), \quad \omega_k = \frac{2\pi k}{NT_s},$$

where $k = 0, 1, \ldots, N-1$, while N denotes a number of samples used for computations. Figure 13 additionally shows Bode-magnitude diagram of transfer function (12) obtained for particular feedforward methods applied in the control system. Properties revealed by the Bode diagram can be confronted with the time plots presented in Fig. 12.

According to the plots in Fig. 13, both CAI and EAI controllers should yield clearly better closed-loop performance

[3]For $\hat{G}(s)$ we have $B(s) = B^p(s)$, $B^n \equiv 1$.

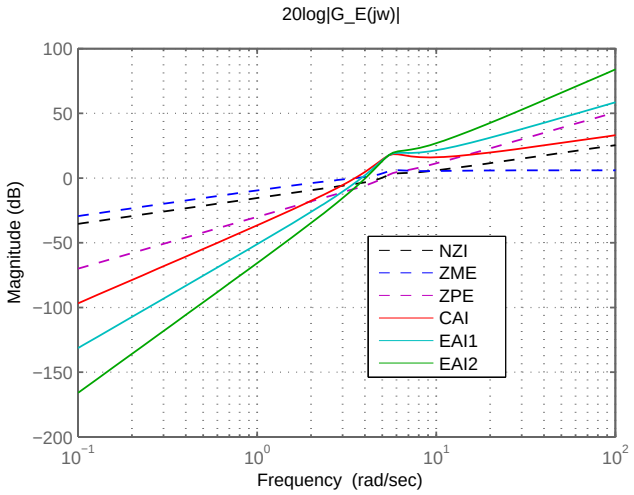

Fig. 13. Frequency responses of the error transfer function (12) computed for plant model $\hat{G}(\bar{j}\omega)$, stabilizing controller $G_R = k_p = 0.1$ and various types of feedforward controllers $G_{\mathrm{FF}}(\bar{j}\omega)$.

for $\omega_d = 1\,\mathrm{rad/s}$ when compared to the classical methods. This prediction is confirmed by the upper time-plots in Fig. 12 and by values of quality functional in Table II. Relative improvement of tracking performance comparing CAI and EAI1 controllers is small in this case. Further practical improvement by application of EAI2 controller seems questionable. One can explain the above effects by the low signal-to-noise ratio reached in this case (values in Table II denoted by a star mark are highly uncertain), by the plant model uncertainty, and by the small value of weight p_4 which does not contribute much relative to other terms present in signal $u_{\mathrm{FF}}^{\mathrm{EAI2}}$.

For the reference frequency $\omega_d = 2\,\mathrm{rad/s}$, it is expected upon the plot in Fig. 13 that CAI controller can provide tracking performance comparable to the ZPE method. Evident improvement should be seen only after application of EAI controllers. These expectations are confirmed by the plots in Fig. 12 and by values of the performance index in Table II. Again, a relative tracking accuracy improvement obtained with EAI2 control law seems to be rather slight when compared to the case of EAI1 controller due to similar reasons mentioned above.

VI. CONCLUDING REMARKS

Summarizing, worth to emphasize that the proposed CAI/EAI feedforward controllers have a fixed weighted-linear-combination structure. It means that the form of equation (3) remains the same for all the plants, minimum- and nonminimum-phase, with the same order of dynamics. This property makes the new controllers especially simple for industrial implementations when the current values of a reference trajectory and its time-derivatives are available. If the reference time-derivatives are not available, it is still possible to use CAI/EAI controllers by reconstructing the time-derivatives e.g. with utilization of the so-called robust exact differentiators introduced in [16], [17].

It has been shown that for sufficiently low frequency range a tracking control accuracy attainable with the proposed method

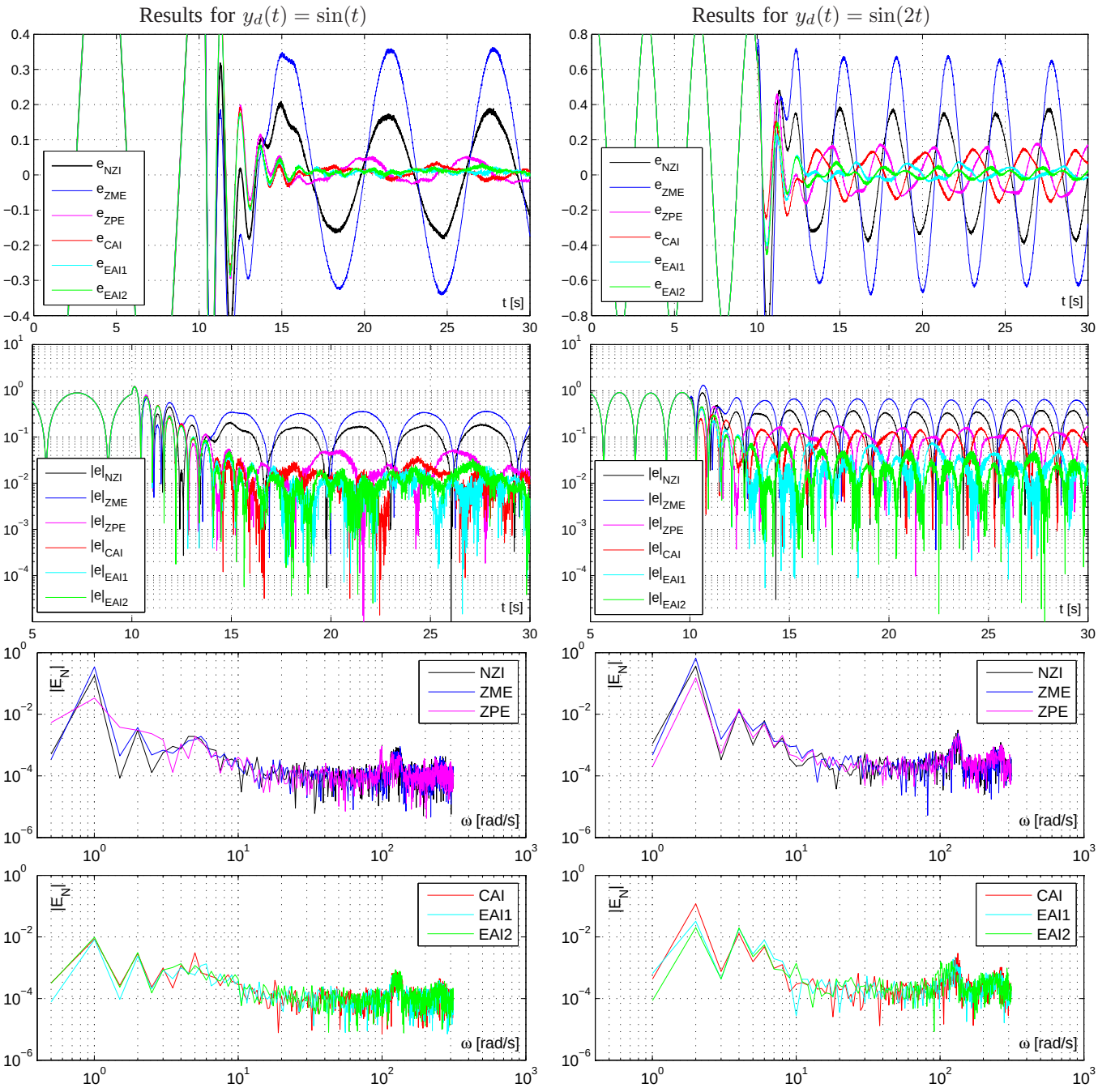

Fig. 12. Plots of tracking errors $e(t)$ in the linear and logarithmic scales together with amplitude spectra $|E_N(\omega)|$ of tracking-error signals obtained on the experimental testbed for the proposed CAI, EAI1, and EAI2 controllers and compared with three classical feedforward controllers NZI, ZME, and ZPE.

can be successively improved by increasing the degree μ of the feedforward controller polynomial. Practical limitation of this reduction generally comes from three main reasons: a lack of knowledge on higher-order time-derivatives of a reference trajectory, a poor quality of a plant model, and the presence of a measurement noise which inherently restricts ability of tracking accuracy improvement below some ultimate level determined by a signal-to-noise ratio. As illustrated in the paper, the XAI controllers designed for sufficiently high polynomial degree μ may outperform the classical approximate-inverse methods when applied to the nonminimum-phase dynamics if a spectrum of a reference trajectory is included in a low-frequency range. Like in the classical feedforward control methods, the particular quantitative tracking improvement attainable with XAI controllers substantially depends on relative locations of poles and zeros of the considered plant dynamics.

At present, the proposed XAI feedforward controllers do not have their counterparts for the plants described by discrete-time models widely used in various applications due to simplicity of their practical utilization. Applicability extension of the proposed feedforward control method for discrete-time systems remains an open research problem.

ACKNOWLEDGMENT

The author is grateful to Eng. T. Jedwabny for the help in preparation of the experimental setup.

REFERENCES

[1] A. P. Aguiar, J. P. Hespanha, and P. V. Kokotović. Path-following for nonminimum phase systems removes performance limitations. *IEEE Trans. Automatic Control*, 50(2):234–239, 2005.

[2] M. R. Buehner and P. M. Young. Perfect tracking for non-minimum phase systems. In *2010 American Control Conf.*, pages 4010–4015, Baltimore, USA, 2010.

[3] J. A. Butterworth, L. Y. Pao, and D. Y. Abramovitch. The effect of nonminimum-phase zero location on the performance of feedforward model-inverse control techniques in discrete-time systems. In *2008 American Control Conf.*, pages 2696–2702, Seattle, USA, 2008.

[4] J. A. Butterworth, L. Y. Pao, and D. Y. Abramovitch. Analysis and comparison of three discrete-time feedforward model-inverse control techniques for nonminimum-phase systems. *Mechatronics*, 22:577–587, 2012.

[5] J. De Caigny, B. Demeulenaere, J. Swevers, and J. De Schutter. Optimal design of spline-based feedforward for trajectory tracking. In *Proc. 2007 American Control Conference*, pages 4524–4529, New York City, USA, 2007.

[6] P. H. Chang and G. R. Cho. Enhanced feedforward control of non-minimum phase systems for tracking predefined trajectory. *Int. J. Control*, 83(13):2440–2452, 2010.

[7] G. M. Clayton, S. Tien, K. K. Leang, Q. Zou, and S. Devasia. A review of feedforward control approaches in nanopositioning for high-speed SPM. *ASME J. Dyn. Sys. Meas. Cont.*, 131:1–19, 2009.

[8] S. Devasia. Should model-based inverse inputs be used as feedforward under plant uncertainty. *IEEE Trans. Control Sys. Techn.*, 47(11):1865–1871, 2002.

[9] M. M. Michałek. Simple causal fixed-structure feedforward control law for general continuous-time LTI SISO systems. In *2014 European Control Conference (ECC)*, pages 61–66, Strasbourg, France, 2014.

[10] H. Garnier and L. Wang (Eds.). *Identification of continuous-time models from sampled data*. Advances in Industrial Control. Springer-Verlag, London, 2008.

[11] E. Gross and M. Tomizuka. Experimental flexible beam tip tracking control with a truncated series approximation to uncancelable inverse dynamics. *IEEE Trans. Control Sys. Techn.*, 2(4):382–391, 1994.

[12] M. Heertjes and D. Bruijnen. MIMO FIR feedforward design for zero error tracking control. In *2014 American Control Conference (ACC)*, pages 2166–2171, Portland, USA, 2014.

[13] J. B. Hoagg and D. S. Bernstein. Nonminimum-phase zeros. Much to do about nothing. *IEEE Control Systems Magazine*, 27(3):45–57, 2007.

[14] A. Karimi, M. Butcher, and R. Longchamp. Model-free precompensator tuning based on the correlation approach. *IEEE Trans. Control Systems Technology*, 16(5):1013–1020, 2008.

[15] K.-S. Kim and Q. Zou. A modeling-free inversion-based iterative feedforward control for precision output tracking of linear time-invariant systems. *IEEE/ASME Trans. Mechatronics*, 18(6):1767–1777, 2013.

[16] A. Levant. Robust exact differentiation via sliding mode technique. *Automatica*, 34(3):379–384, 1998.

[17] A. Levant. Higher-order sliding modes, differentiation and output-feedback control. *Int. J. Control*, 76(9/10):924–941, 2003.

[18] H. Okajima and T. Asai. Performance limitation of tracking control problem for a class of references. *IEEE Trans. Automatic Control*, 56(11):2723–2727, 2011.

[19] H.-S. Park, P.-H. Chang, and D.-Y. Lee. Trajectory planning for the tracking control of systems with unstable zeros. *Mechatronics*, 13:127–139, 2003.

[20] A. Pisano, S. Baev, D. Salimbeni, Y. Shtessel, and E. Usai. A new approach to causal output tracking for non-minimum phase nonlinear systems via combined first/second order sliding mode control. In *2013 European Control Conference (ECC)*, pages 3234–3239, Zürich, Switzerland, 2013.

[21] B. P. Rigney, L. Y. Pao, and D. A. Lawrence. Nonminimum phase dynamic inversion for settle time applications. *IEEE Trans. Control Sys. Technology*, 17(5):989–1005, 2009.

[22] W. Su, L. Qiu, and J. Chen. On performance limitation in tracking a sinusoid. *IEEE Trans. Automatic Control*, 51(8):1320–1325, 2006.

[23] D. Torfs and J. De Schutter. Optimal feedforward prefilter with frequency domain specification for nonminimum phase systems. *J. Dynamic Systems, Measurement, and Control*, 118:791–795, 1996.

[24] D. E. Torfs, R. Vuerinckx, J. Swevers, and J. Schoukens. Comparison of two feedforward design methods aiming at accurate trajectory tracking of the end point of a flexible robot arm. *IEEE Trans. Control Systems Technology*, 6(1):2–14, 1998.

[25] S. van der Meulen, R. Tousain, and O. Bosgra. Fixed structure feedforward controller tuning exploiting iterative trials, applied to a high-precision electromechanical servo system. In *Proc. the 2007 American Control Conference (ACC)*, pages 4033–4039, New York City, USA, 2007.

[26] Q. Zou. Optimal preview-based stable-inversion for output tracking of nonminimum-phase linear systems. *Automatica*, 45:230–237, 2009.

[27] Q. Zou and S. Devasia. Preview-based optimal inversion for output tracking: application to scanning tunneling microscopy. *IEEE Trans. Control Sys. Techn.*, 12(3):375–386, 2004.